



**HAL**  
open science

## **Spectral induced polarization of heterogeneous non-consolidated clays**

A Mendieta, A Mainault, P Leroy, D Jougnot

► **To cite this version:**

A Mendieta, A Mainault, P Leroy, D Jougnot. Spectral induced polarization of heterogeneous non-consolidated clays. *Geophysical Journal International*, In press, <10.1093/gji/ggac466>. <hal-03879461>

**HAL Id: hal-03879461**

**<https://hal.sorbonne-universite.fr/hal-03879461v1>**

Submitted on 30 Nov 2022

**HAL** is a multi-disciplinary open access archive for the deposit and dissemination of scientific research documents, whether they are published or not. The documents may come from teaching and research institutions in France or abroad, or from public or private research centers.

L'archive ouverte pluridisciplinaire **HAL**, est destinée au dépôt et à la diffusion de documents scientifiques de niveau recherche, publiés ou non, émanant des établissements d'enseignement et de recherche français ou étrangers, des laboratoires publics ou privés.



HAL Authorization

1                    **Spectral induced polarization of heterogeneous**  
2                    **non-consolidated clays**

3                    **A. Mendieta<sup>1</sup>, A. Mainault<sup>1</sup>, P. Leroy<sup>2</sup>, and D. Jougnot<sup>1</sup>**

4                    <sup>1</sup>Sorbonne Université, CNRS, EPHE, UMR 7619 METIS, 75005 Paris, France

5                    <sup>2</sup>BRGM, Department of Water, Environment, Processes and Analysis, 45100 Orléans, France

6                    **Key Points:**

- 7                    • Hydrogeophysics  
8                    • Electrical properties  
9                    • Numerical modelling  
10                    • Electrical anisotropy  
11                    • Electromagnetic theory

---

Corresponding author: Aida Mendieta, [aida.mendieta.tenorio@sorbonne-universite.fr](mailto:aida.mendieta.tenorio@sorbonne-universite.fr)

## Abstract

Clays are ubiquitously located in the Earth's near surface and have a high impact on the subsurface permeability. Most geo-electrical characterizations of clays do not take into account the heterogeneous nature of clay geological media. We want to better understand the influence of heterogeneities on the geo-electrical signature, thus we collected a dataset of spectral induced polarization (SIP) of artificial heterogeneous non-consolidated clay samples. The samples are made of illite and red montmorillonite in a parallel and perpendicular disposition (with respect to the applied electric field). Another sample is a homogeneous mixture composed of the same volumetric fraction of illite and red montmorillonite. For all the samples, the polarization is dominated by the red montmorillonite, given by the shape of the spectra (presence or lack of a peak at a particular frequency). We compared the experimental data with classical mixing laws and complex conductance network models to test how to better predict the SIP signature of such mixtures when the SIP spectra of the two components are known. The real conductivity is better predicted by the mixing laws, but the shape of the spectra (presence of polarization peaks at particular frequencies) is best predicted by the conductance network models. This study is a step forward towards a better characterization of heterogeneous clay systems using SIP.

## 1 Introduction

Clayey material exists in a variety of geologic formations and at various scales, from cap rocks to clay lenses or clay fractions in soils. Most laboratory geo-electrical characterizations of clays are done for a homogeneous mixture of clays, a mixture of sand and clays, or a clayrock sample from a particular geological formation (e.g., Cosenza et al., 2008; Ghorbani et al., 2009; Jougnot et al., 2010; Breede et al., 2012; Okay et al., 2014). However, most clay systems are heterogeneous and/or anisotropic (e.g., Wenk et al., 2008; Revil et al., 2013; Woodruff et al., 2014; Al-Hazaimay et al., 2016), thus these laboratory characterizations can fall short to predict the electrical signature of a heterogeneous and/or anisotropic clay system. There is a lack of geo-electrical laboratory experiments that better represent the complexity of clay systems. Additionally, there is a need to bridge the knowledge gaps between scales (clay sample to clay system). Moreover, there is a lack in our understanding of the electrical conduction and polarization phenomena at

43 the mesoscopic scale, that is a scale larger than the typical pore size but smaller than  
44 the volume investigated by geophysical measurements (see Jougnot, 2020).

45 Physical properties of mixtures (hydraulic, electrical, elastic, among others) can be pre-  
46 dicted with the use of mixing laws, such as Voigt (1910), Reuss (1929), and the self-consistent  
47 approach (Hashin, 1968). Mixing laws make use of a volumetric weighted average of the  
48 electrical properties of the individual components, without taking into account partic-  
49 ular geometries. According to Knight & Endres (2005), simple approaches as these are  
50 able to properly predict the resulting electrical property from a sample with the elec-  
51 trical field in a parallel or perpendicular orientation with respect to its layering. Mix-  
52 ing models are a traditional, yet still effective approach used in geophysics (e.g., Berry-  
53 man, 1995; Renard & de Marsily, 1997; Jougnot et al., 2018).

54 Another approach to bridge the scales in the geosciences is through pore network mod-  
55 eling (e.g., Bernabe, 1995; Day-Lewis et al., 2017; Jougnot et al., 2019). This approach  
56 when adapted to the electrical properties of media leads to impedance or conductance  
57 networks (e.g., Madden, 1976; Stebner et al., 2017). Mainault et al. (2018b), have related  
58 the pore properties (like pore radius) to electrical properties through phenomenological  
59 models, like a Pelton model (Pelton et al., 1978). In this study, we use the measured spec-  
60 tra for individual clays (see Mendieta et al., 2021) as input of each impedance of the net-  
61 work.

62 In Mendieta et al. (2021), five types of clays were studied at different salinities. Here,  
63 we use two of those types of clays, illite and red montmorillonite. In this work, we built  
64 synthetic samples in parallel (longitudinal disposition), series (transversal disposition),  
65 and homogeneous mixture configurations of both types of clays. We used complex con-  
66 ductance network modeling and mixing laws to predict the complex electrical conduc-  
67 tivity response of the red montmorillonite and illite (initially at 0.01 M of NaCl) (see Mendi-  
68 eta et al., 2021). In this study, we consider extreme bounds of mixtures (Voigt and Reuss  
69 models) and heterogeneities, taking a step forward towards a better characterization of  
70 complex clay systems in situ.

71 To our knowledge, this use of mixing laws to describe the complex conductivity (real and  
72 imaginary parts) of clay mixtures from their pure components is novel. Indeed, tradi-  
73 tionally, these formulas are used for the magnitude of the electrical conductivity only (e.g.,

Berryman, 1995). Similarly, the use of complex conductance networks to predict the electrical signature of laboratory measurements, particularly at this scale is novel.

## 2 Theory

### 2.1 Spectral Induced Polarization

SIP is a geophysical method that consists in injecting a sinusoidal-shaped electrical current into a rock sample and measuring the resulting electric potential difference and the phase-lag between the injected current and the potential difference, at different finite frequencies (mHz-kHz). The voltage-to-current ratio yields information about the electrical impedance of the rock sample, while the phase-lag ( $\varphi$ , in rad) informs about the capacity of the rock sample to reversibly store electrical charges (e.g., Revil, 2012). With the proper geometrical factor, we can obtain the electrical resistivity ( $\rho$ , in  $\Omega$  m) or its inverse, the conductivity ( $\sigma$ , in  $S\ m^{-1}$ ) of the sample. Generally, the complex electrical conductivity ( $\sigma^*(\omega)$ , or the complex resistivity  $\rho^*(\omega)$ ) is frequency dependent and can be presented as:

$$\frac{1}{\rho^*(\omega)} = \sigma^*(\omega) = |\sigma|e^{i\varphi} = \sigma' + i\sigma'', \quad (1)$$

where  $\omega$  is the angular frequency ( $rad\ s^{-1}$ ),  $i = \sqrt{-1}$  represents the imaginary unit,  $|\sigma|$  is the amplitude of the measured signature ( $S\ m^{-1}$ ),  $\sigma'$  ( $S\ m^{-1}$ ) is the real component of the electrical conductivity, and  $\sigma''$  ( $S\ m^{-1}$ ) is the imaginary component. The relation between  $\omega$  and the frequency ( $f$ , Hz) is  $\omega = 2\pi f$ .

In the frequency range from the mHz to the kHz there is thought to be three polarization mechanisms (see Kemna et al., 2012; Loewer et al., 2017) giving rise to the measured polarization: the membrane polarization mechanism, the electrical double layer (EDL) mechanism, and the Maxwell-Wagner polarization mechanism. The membrane polarization mechanism happens at the lowest frequencies (mHz range) and arises from blockage of ions in pore throats (see Bückner & Hördt, 2013a,b). The EDL polarizes in the mid-frequency range (in the Hz range) due to the polarization of the Stern and diffuse layers around minerals surrounded by an electrolyte (see Leroy et al., 2017; Bückner et al., 2019). Finally, at the highest frequencies (kHz range) the Maxwell-Wagner po-

101 larization mechanism takes place at the interfaces of different phases in direct contact  
 102 with each other (see Loewer et al., 2017).

## 103 2.2 Mixing laws

104 There are multiple ways to calculate the electrical signature of heterogeneous or  
 105 homogeneous mixtures. Commonly used mixing laws in geophysics (for electric, elastic,  
 106 magnetic, among many other physical properties) are the Voigt (1910), Reuss (1929),  
 107 and self-consistent approach (Hashin, 1968) to mixtures (see Renard & de Marsily, 1997,  
 108 for a review on permeability), the volume averaging approach (Pride, 1994; Revil et al.,  
 109 2007), and the differential effective medium theory (e.g., de Lima & Sharma, 1992; Cosenza  
 110 et al., 2008). With the differential medium theory, the effect of inclusions with their own  
 111 electrical properties is added to a background with different electrical properties. The  
 112 geometry of the whole mixture is modified by adding the inclusions iteratively, until a  
 113 geometrical requirement is met, thus calculating the electrical property of the whole mix-  
 114 ture. For the volume-averaging approach, the governing and constitutive equations of  
 115 interest (e.g. Maxwell laws for electrical properties) are averaged in a representative el-  
 116 elementary volume. Mixing laws are a simple, yet effective approach to calculate the re-  
 117 sulting electrical properties from a volumetric weighted average of the individual com-  
 118 ponents. We decided to use mixing laws due to their simplicity, yet effectiveness.

119 Here, we focus on the Voigt, Reuss, and self-consistent theory. For a mixture made of  
 120 two materials, the resulting electrical signature will be bound (minimum and maximum)  
 121 by the electrical signature of the individual materials. When the mixture is disposed in  
 122 parallel (i.e., considering an analogous electrical circuit), we can use the Voigt (1910) ap-  
 123 proach to calculate the resulting electrical signature, that is:

$$\sigma_V^* = c\sigma_1^* + (1 - c)\sigma_2^*, \quad (2)$$

124 where,  $\sigma_V^*$  represents the complex electrical conductivity of the mixture disposed par-  
 125 allel to the applied electrical field,  $\sigma_1^*$  represents the complex electrical conductivity of  
 126 the first material, and  $\sigma_2^*$  of the second material, and  $c$  is the volumetric proportion of  
 127 material 1 with respect of the whole volume of the mixture. For a series disposition (per-  
 128 pendicular to the applied electrical field), we use the Reuss (1929) approach, that is:

$$\sigma_R^* = \left( \frac{c}{\sigma_1^*} + \frac{1-c}{\sigma_2^*} \right)^{-1}, \quad (3)$$

129 where  $\sigma_R^*$  is the complex electrical conductivity of the mixture disposed in series. Finally,  
 130 when there is a homogeneous mixture of two materials, we can use the self-consistent  
 131 (Hashin, 1968) approach, that is:

$$\sigma_{SC}^* = \sigma_2^* + \frac{3c\sigma_2^*}{3\sigma_2^* + (1-c)(\sigma_1^* - \sigma_2^*)}(\sigma_1^* - \sigma_2^*) \quad (4)$$

132 where  $\sigma_{SC}^*$  is the complex electrical conductivity of the homogeneous mixture of two ma-  
 133 terials. In our case  $c = 0.5$  for all mixtures, that is for equations 2, 3, and 4. Note that  
 134 when  $c = 0.5$ , equation 2 becomes a simple arithmetic mean, and equation 3 becomes  
 135 a harmonic mean. These expressions have previously been used for the amplitude of the  
 136 electrical conductivity (e.g., Berryman, 1995), not for the entire complex conductivity  
 137 (that is the real and imaginary part) in SIP laboratory measurements. It is worth men-  
 138 tioning that Kenkel et al. (2012) created a forward model for anisotropic media using  
 139 mixing laws with complex conductivity to better understand field measurements of anisotropic  
 140 media.

### 141 **2.3 Complex conductance network modeling**

142 To simulate the SIP signature of the clay mixtures, we additionally used complex  
 143 conductance networks (see for instance Mainault et al., 2017; Mainault, 2018a; Mainault  
 144 et al., 2018b, 2021). We designed a network on a regular 2D mesh (see the example given  
 145 in Fig. 1). Each link of the network consists of a given complex conductance. By apply-  
 146 ing Kirchhoff's law (1845), we obtain a linear equation expressing the current continu-  
 147 ity at each node of the network. Replacing the current in a given link by the product  
 148 of the complex conductance of this link and the electrical potential difference between  
 149 the two nodes delimiting this link, and applying the boundary conditions (i.e., the po-  
 150 tential is equal to  $V_0 e^{i\omega t}$ , with  $V_0 = 1V$  at the bottom and 0 at top, with no flux on  
 151 the lateral faces, see Fig. 1), we can obtain a linear system that is solved for each an-  
 152 gular frequency  $\omega$  in order to get the potentials at the nodes. For more detail see Mainault  
 153 et al., 2017, section 2.2. We impose a potential value at the top and bottom boundaries  
 154 and deduce a flux. It is then straightforward to deduce the ratio of the potential differ-  
 155 ence applied between the two end faces to the computed total inflowing/outflowing cur-

156 rent, as well as the phase-shift between these two quantities (please note that the full  
 157 derivation for a square mesh can be found in Mainault et al., 2017, corrected by Mainault,  
 158 2018a). In the case of an illite and red montmorillonite mixture, we use the impedance  
 159 spectra reported in Mendieta et al. (2021) for illite and red montmorillonite at 0.01 M  
 160 NaCl (presented in Fig. 3). Please note that this type of modeling can be done for dif-  
 161 ferent types of connectivity (e.g., triangular, rectangular, or hexagonal mesh).

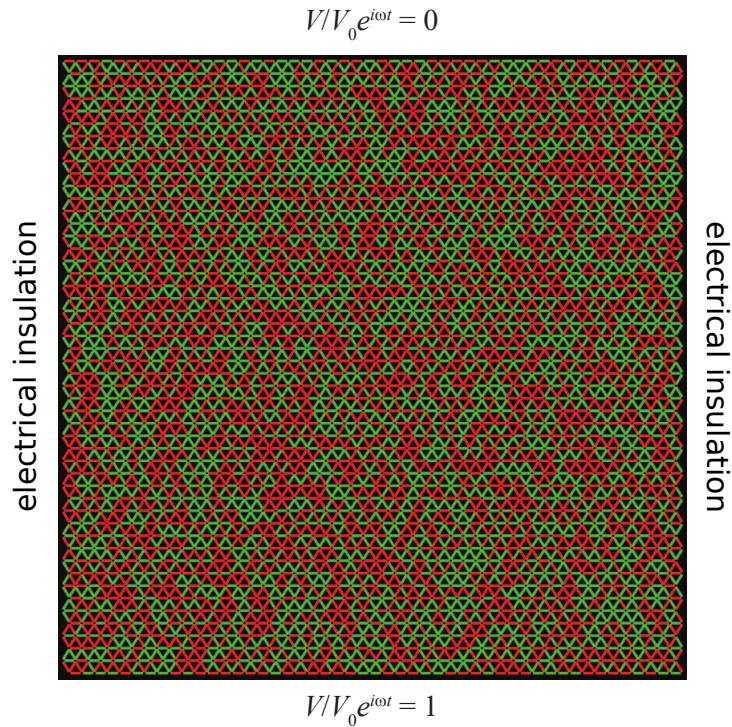


**Figure 1.** 50x50 triangular complex conductance network simulating a random homogeneous mixture of illite and red montmorillonite. The green links correspond to illite, the red ones to red montmorillonite.

### 162 3 Materials and Methods

#### 163 3.1 Materials

164 The SIP responses of four (red and green montmorillonite, illite and kaolinite) types  
 165 of clays have been characterized individually at different salinities in Mendieta et al. (2021).  
 166 Based on their results, we used two clay types with a completely different behaviour (with  
 167 respect to their electrical signature): illite and red montmorillonite. We also decided to  
 168 use an initial salinity that would show a significant difference between both clay types.

169 An excessively high salinity would have created extremely conductive clay samples, yield-  
170 ing SIP data with high noise, and an excessively low salinity sample would have created  
171 important non-equilibrium in the pore-water chemistry (possible ion release from the in-  
172 terlayer space of clay tactoids as discussed in Mendieta et al., 2021). Thus we decided  
173 to use an initial salinity of  $10^{-2}$  M of NaCl. As described in Mendieta et al. (2021), the  
174 clay samples follow an evaporation period, thus the salinity of the SIP measured clay sam-  
175 ple is in the same order of magnitude as the initial salinity but not exactly the same.

176 A detailed description and analysis of the clays used in this study, with a detailed ex-  
177 planation of the laboratory protocol is presented in Mendieta et al. (2021). We will how-  
178 ever, briefly describe the used materials and laboratory protocol.

179 In the present study we used two types of non-pure clays, a red montmorillonite and an  
180 illite. A chemical analysis of the clay samples shows that the red montmorillonite sam-  
181 ple is made of: 66% smectite, 11% quartz, 18% microcline, 3% albite, and 1% magnetite.  
182 The illite sample is made of: 67% illite, 10% kaolinite, 10% microcline, and 12% calcite.  
183 The measured cationic exchange capacity (CEC) values are 135 meq/100 g for the red  
184 montmorillonite sample, and 47 meq/100 g for the illite sample. Finally, the measured  
185 specific surface area through the Brunauer-Emmett-Teller (BET) method is  $71.09 \text{ m}^2/\text{g}$   
186 for the red montmorillonite sample, and  $101.60 \text{ m}^2/\text{g}$  for the illite sample. It is worth  
187 noting that the use of the BET method has proven to not be optimal for smectites, as  
188 the BET method is unable to probe the interlayer space. Specific surface area values pro-  
189 posed in the literature for smectites are in the range of  $390\text{-}780 \text{ m}^2/\text{g}$  (see Tournassat  
190 et al., 2013).

### 191 **3.2 Laboratory protocol**

192 In this study we prepared three heterogeneous mixtures, and one homogeneous mix-  
193 ture of red montmorillonite and illite. For the heterogeneous mixtures, we located the  
194 individual clay types in two different arrangements: a transversal (Fig. 2b, or series ar-  
195 rangement) and longitudinal arrangements (Figs 2c and d, or parallel arrangements). We  
196 aimed at creating a 50-50% volume ratio, for each type of clay. For the creation of the  
197 heterogeneous mixtures, we created individual clay samples of illite and red montmoril-  
198 lonite, following the protocol proposed by Mendieta et al. (2021) (see their subsection  
199 3.2). For the homogeneous mixture (Fig. 2a), there are extra previous steps in the lab-

200 oratory protocol. This laboratory protocol consists in: a combination of clay powder and  
 201 the aqueous solution, a period of at least 24 h for saturation and equilibrium of the mix-  
 202 ture, mixing of the sample with an electric drill, disposition of the clay sample on top  
 203 of a polyurethane foam until the correct water content is achieved through evaporation,  
 204 the placement of the clay sample inside the sample holder for the SIP measurements, and  
 205 finally the drying of the clay sample. For the homogeneous mixture, the extra previous  
 206 steps are: mixing the dry clay powders of illite and montmorillonite with an electrical  
 207 drill. Using the same mass proportions as in the 50-50% volumetric heterogeneous mix-  
 208 tures.

209 For the SIP measurements, all clay samples are placed in a cylindrical sample holder,  
 210 the injecting electrodes are located on the sides of the cylinder, and the measuring elec-  
 211 trodes are located on top of the cylinder casing (Fig. 2e). This is why we measured the  
 212 SIP signature of two longitudinal heterogeneous mixtures, once the upper half (in con-  
 213 tact with the measuring electrodes) was filled with illite (Fig. 2c), and once with red mont-  
 214 morillonite (Fig. 2d).

### 215 3.3 SIP measurement

216 We used the SIP-FUCHS III equipment (Radic Research, [www.radic-research.de](http://www.radic-research.de))  
 217 for the SIP measurements. See Fig. 2(e) for a sketch of the SIP measuring setup. We  
 218 utilized Cu-CuSO<sub>4</sub> non-polarizable electrodes as electric potential measuring electrodes.  
 219 Indeed, in order to build the non-polarizable electrodes, we followed the procedure pre-  
 220 sented in Kremer et al. (2016), that is we filled a plastic tube with a gelified CuSO<sub>4</sub> so-  
 221 lution. The dimensions of the electrodes are 5 mm diameter and around 10 cm in height.  
 222 The bottom of the electrodes is plugged by a ceramic porous filter, and on the top by  
 223 a rubber plug with an inserted copper wire. For the injecting electrodes we used two stain-  
 224 less steel cylinders that also served as covers of the sample holder. We made use of a four-  
 225 electrode system for the SIP measurements, as according to Kemna et al. (2012) using  
 226 a two-electrode system introduces unacceptably large errors in the measurement in our  
 227 frequency range of interest. As presented in Fig. 2(e) the length of the sample holder  
 228 is of 229.32 mm with a diameter of 43.20 mm. The electrodes are equally separated; we  
 229 chose this configuration based on the recommendations presented in Zimmermann et al.  
 230 (2008). We measured the SIP signature from 1 mHz to 20 kHz twice, separated by around

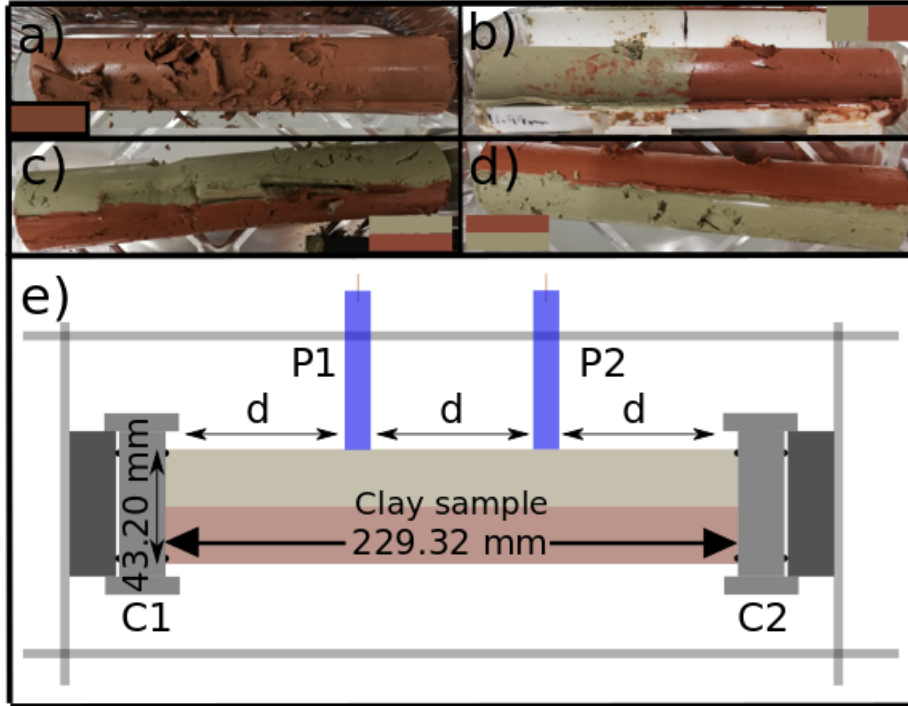


**Figure 2.** Different clay samples prepared in the laboratory. a) A homogeneous mixture of illite and red montmorillonite, b) heterogeneous-transversal mixture of illite and red montmorillonite, c) longitudinal mixture with illite on the side of the measuring electrodes, and d) longitudinal mixture with red montmorillonite on the side of the measuring electrodes. Note that these pictures correspond to the clay samples after taking them out of the sample holder. e) Sketch of the clay sample holder and external structure (grey lines), where C1 and C2 are the injecting electrodes, P1 and P2 are the potential electrodes. Note that this is merely a sketch of the SIP measurement setup and is not at a 1:1 scale.

231 24h. The SIP data we present in this work correspond to the second measurement, as  
 232 the system is mostly equilibrated and the signature is then more stable.

### 233 3.4 Complex conductance network models

234 The principles of the complex conductance network models are explained in sec-  
 235 tion 2.3. Fig. 1 represents a homogeneous mix of illite and red montmorillonite with a  
 236 triangular mesh. Additionally, we modeled a complex conductance network where the  
 237 top half was solely illite and the bottom solely red montmorillonite. We also modeled

238 a complex conductance network with the right half corresponding to illite, and the left  
 239 half corresponding to red montmorillonite. It is worth mentioning that the order of the  
 240 location (which clay is located in which half) is irrelevant, as in this model there are no  
 241 point measurements for the electric potential (opposite to laboratory measurements). For  
 242 instance, locating the illite on the top or bottom will not alter the results, as the con-  
 243 ductance network will yield the resulting electric potential difference of the system as  
 244 a whole. Note that we performed the calculations for a triangular mesh (as shown in Fig. 1),  
 245 but also for a rectangular and hexagonal mesh. The results of the rectangular and hexag-  
 246 onal meshes are presented in the supplementary information file. Overall, the triangu-  
 247 lar mesh proves to be the best option because it has the highest connectivity among the  
 248 rectangular, hexagonal, and triangular meshes. The triangular mesh (highest connectiv-  
 249 ity) presents the best fit between data and models, this can be interpreted as our sam-  
 250 ple (non-consolidated clays) having high connectivity themselves (see supplementary in-  
 251 formation, Fig. S3). Additionally, the meshes used in this contribution had a  $50 \times 50$   
 252 size. Please note that after some tests it appears that the mesh size of  $50 \times 50$  is suf-  
 253 ficient to converge to a unique response. For additional information, see Mainault et al.  
 254 (2017), and supplementary information (Fig. S4).

## 255 4 Results

### 256 4.1 Complex conductivity measurements

257 The results of the SIP measurements of the homogeneous and heterogeneous mix-  
 258 tures are presented in Fig. 3. Note that the datasets of the individual clay types, illite  
 259 and red montmorillonite, have been added for reference, these data were taken from Mendi-  
 260 eta et al. (2021). From the results we can see that all mixtures of illite and red mont-  
 261 morillonite fall in between the data points of illite and red montmorillonite, which is ex-  
 262 pected. Here, we measured the SIP signature of a homogeneous mixture of illite and red  
 263 montmorillonite, and three heterogeneous mixtures placed in a longitudinal (parallel)  
 264 and transversal (series) manner. For the longitudinal set-ups, we conducted two mea-  
 265 surements, one locating the illite on the top portion of the sample holder (near the mea-  
 266 suring electrodes, see Fig. 2c) and the second with the red montmorillonite on top (see  
 267 Fig. 2d). We can see that these longitudinal measurements do not match perfectly, and  
 268 that makes sense; we do not have the same sensitivity immediately at 1 or 2 cm below  
 269 the measuring electrodes. However, we see that the longitudinal mixture with the illite

270 on the top portion of the sample holder, is not identical to the measurement of solely  
 271 illite, that means that the longitudinal mixture with the illite on top is still affected by  
 272 the red montmorillonite below. If we take a look at Fig. 3, we verify that the transversal  
 273 mixture is in fact closer in both value and shape to the individual illite than the longitudinal  
 274 mixture with illite on the top. By shape, we refer to the presence or lack thereof  
 275 a peak in the phase or imaginary conductivity near 10 Hz. This also proves that the red  
 276 montmorillonite in the longitudinal mixture with illite on the top affects the SIP signature  
 277 (i.e. the SIP measurement is sensitive to the red montmorillonite on the bottom of  
 278 the sample holder).

279 The bounds of the electrical in-phase conductivities of the mixtures are the electrical con-  
 280 ductivities of both illite and red montmorillonite (see Fig. 3). The electrical conductiv-  
 281 ities at 1.46 Hz of the red montmorillonite and illite are  $0.39 \text{ S m}^{-1}$  and  $0.16 \text{ S m}^{-1}$ , re-  
 282 spectively. The corresponding electrical conductivity values of the mixtures at 1.46 Hz  
 283 are:  $0.22 \text{ S m}^{-1}$  (transversal arrangement),  $0.24 \text{ S m}^{-1}$  (longitudinal arrangement with  
 284 the illite on the top portion of the sample holder),  $0.28 \text{ S m}^{-1}$  (longitudinal arrangement  
 285 with the red montmorillonite on the top portion of the sample holder), and  $0.26 \text{ S m}^{-1}$   
 286 (for the homogeneous arrangement). We verify that all mixtures fall between the bounds.  
 287 For the phase, in the lower frequencies (1 mHz to 5.9 Hz) all the spectra resemble. How-  
 288 ever in the higher frequencies (above 5.9 Hz), we can see a clear difference between the  
 289 spectra of each mixture. At 750 Hz, the phase of the illite sample is of 4.7 mrad, and of  
 290 the red montmorillonite is 14.8 mrad. The transversal dataset (black dots) is the one that  
 291 is closer to the value of the phase of the illite and it is 10.8 mrad. The rest of the mix-  
 292 tures are quite closer in value to the red montmorillonite.

293 Note that the mixtures and the individual complex conductivity spectra of illite and red  
 294 montmorillonite were collected at different temperatures. The illite SIP data were col-  
 295 lected at a temperature of around  $21.9 \text{ }^\circ\text{C}$ , and the montmorillonite SIP data were col-  
 296 lected at around  $23.1 \text{ }^\circ\text{C}$ . The heterogeneity SIP dataset was collected at around  $18.9$   
 297  $^\circ\text{C}$ . We corrected the heterogeneity dataset to a  $22.5 \text{ }^\circ\text{C}$  temperature. We used the tem-  
 298 perature correction proposed by Hayley et al. (2007). The maximum percentage change  
 299 between the measured and the temperature corrected conductivity for all datasets is of  
 300 8.8%. It is worth mentioning that we only corrected the conductivity magnitude, because  
 301 to the best of our knowledge there is not a temperature correcting procedure for the phase.  
 302 Although it has been pointed out that temperature influences the complex conductiv-

303 ity of a geo-material (e.g., Zisser et al., 2010; Bairlein et al., 2016; Iravani et al., 2020),  
 304 there is still a need to find a petrophysical law or relation to correct for it (see Kemna  
 305 et al., 2012).

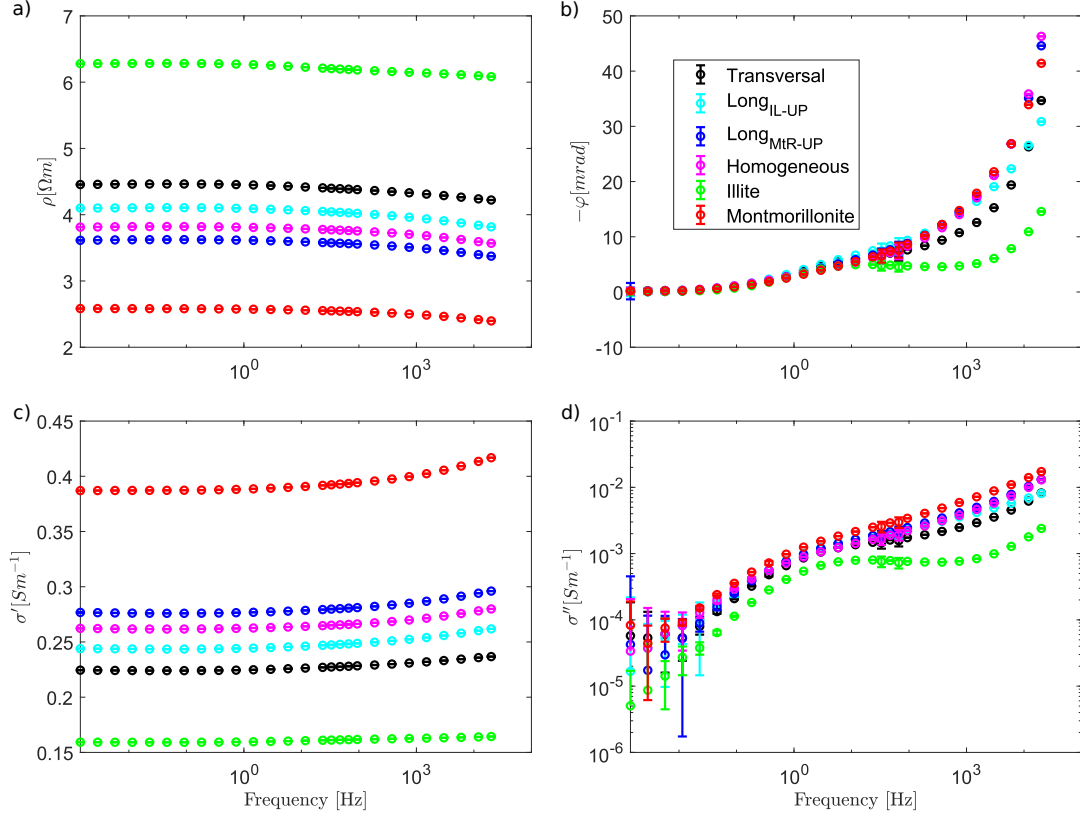


**Figure 3.** SIP data, as a) amplitude, b) phase, c) real component and d) imaginary components of the complex conductivity. The illite and red montmorillonite clay samples have been taken from Mendieta et al. (2021). The rest of the datasets here presented are a homogeneous mixture of illite and red montmorillonite, as well as three heterogeneous mixtures: a transversal mixture (series), and two longitudinal mixtures (parallel), one with illite in contact with the measuring electrodes (Long<sub>IL-UP</sub>), and one with red montmorillonite (Long<sub>MtR-UP</sub>).

306 **4.2 Complex conductance network modeling results**

307 As mentioned in section 3.4, we modeled the complex conductivity of three differ-  
 308 ent mixtures: a homogeneous mixture, a transversal-heterogeneous mixture, and a longitudinal-  
 309 heterogeneous mixture. Note that for the complex conductance network models we can-  
 310 not obtain a model for illite or red montmorillonite on the side of the measuring elec-

trodes, because for complex conductance network models, there is no point measure. In the mesh, the side on which each clay is located does not affect the end result of the model. For each type of mixture we considered three types of mesh for the numerical modeling (with a different connectivity each): a rectangular, a hexagonal, and a triangular mesh. In this contribution we will only present the simulations results using the triangular mesh, the simulations using other meshes are presented in the supplementary material. In Fig. 4 we present the SIP data overlaid by the results of the complex conductance network models; that is the real and imaginary part of the conductivity (Figs 4a and b, respectively), and the normalized real and imaginary conductivities (Figs 4c and d, respectively). We have normalized the spectra by the conductivity value at 1.46 Hz. We chose the closest value to 1 Hz, as this is a widely used value in geophysics (e.g., Zanetti et al., 2011).

Both model and data (Fig. 4) resemble more the red montmorillonite than the illite complex conductivity spectra, in shape (i.e. lack of a peak in the phase and imaginary conductivity near 10 Hz). It appears that the red montmorillonite affects more the resulting polarization than the illite in a mixture with equal proportions, whether it is a homogeneous mixture or a heterogeneous one. We also notice that the fit is not perfect between the prediction of the triangular conductance network model and the data; it is possible that the difference is due to 3D effects while the conductance network is in 2D. However, for the whole spectra the difference between model and data, for the real conductivity remains below  $0.01 \text{ S m}^{-1}$ . Al-Hazaimay et al. (2016) measure the SIP signature of two anisotropic systems and perform a numerical model. They add a correction factor to be able to compare 2D anisotropic models to real anisotropic systems measured in the laboratory. Due to our measuring setup, we are unable to apply such correction.

### 4.3 Comparison with mixing laws

We additionally modeled the SIP signature of the different mixtures using the mixing laws proposed by Voigt (1910), Reuss (1929) and Hashin (1968). In Fig. 5, we confront the SIP data versus these models. Note that we present a Voigt<sub>IL-UP</sub> and a Voigt<sub>MtR-UP</sub> model. We use bulkhead connectors in order to fix the measuring electrodes in the sample holder during the SIP measurement. For this reason on the half-cylinder side next to the electrodes a small volume corresponding to the nut of the bulkhead connector must be subtracted, that is both halves do not have equal volume. The volume used by the bulkhead connector is  $0.184 \text{ cm}^3$ . For the case of both volume fractions being equal  $c =$

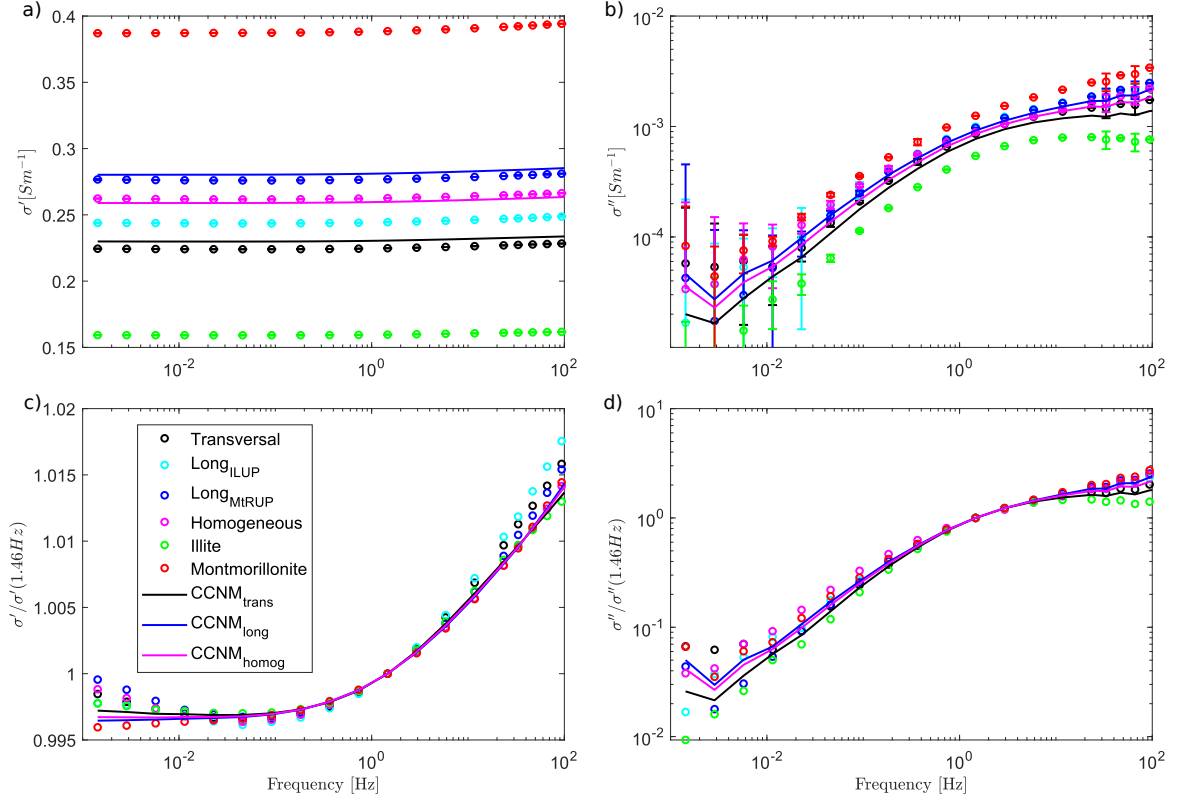


**Figure 4.** a) Real conductivity measurements and conductance network models, b) imaginary conductivity measurements overlain by the conductance network models, c) normalized real conductivity of the measurements and conductance network models, and d) normalized imaginary conductivity of the measurements and conductance network models of the illite and red montmorillonite mixtures. Long<sub>IL-UP</sub> and Long<sub>MtR-UP</sub> refer to the longitudinal mixtures (parallel), with illite and red montmorillonite near the potential electrodes, respectively. CCNM-trans, long, and homog refer to the complex conductance network models using the transversal, longitudinal and homogeneous arrangements, respectively.

343 0.5, but when the electrode volume has been removed, we obtain  $c = 0.5005$  (see equa-  
 344 tion 2). Therefore, we used Voigt's model for an illite in the top half (IL-UP, in contact  
 345 with the potential electrodes), and a model with the red montmorillonite on the top half  
 346 (MtR-UP). In figure 5, we present these models with a different  $c$  value as Voigt<sub>IL-UP</sub>  
 347 and Voigt<sub>MtR-UP</sub>, both are too close to each other and that it is impossible to discern  
 348 the difference a  $c$  value of 0.0005 makes in the model. In general for the mixing laws, we  
 349 see that overall the modeled values are affected by both members of the mixtures, the  
 350 red montmorillonite and illite (see Figs 5a and b). As to the shape of the spectra (lack

351 of a peak near 10 Hz for the imaginary part of the conductivity), if we take a look at Figs  
 352 5c and d, we could interpret that the shape of the curve of both Voigt's models are more  
 353 affected by the red montmorillonite content, and so are the data. That is, we are not able  
 354 to properly model the dataset with illite in the top half (illite in contact with the po-  
 355 tential electrodes). On the other hand, both Reuss and self-consistent models seem to  
 356 be affected by both the illite and red montmorillonite content, in the shape of their spec-  
 357 tra (closer to presenting a peak near 10 Hz). However, the corresponding datasets do not  
 358 seem to follow the same trend as for the shape of the spectra. It is worth mentioning that  
 359 these measurements contain errors that are inherent to the nature of experimental data.

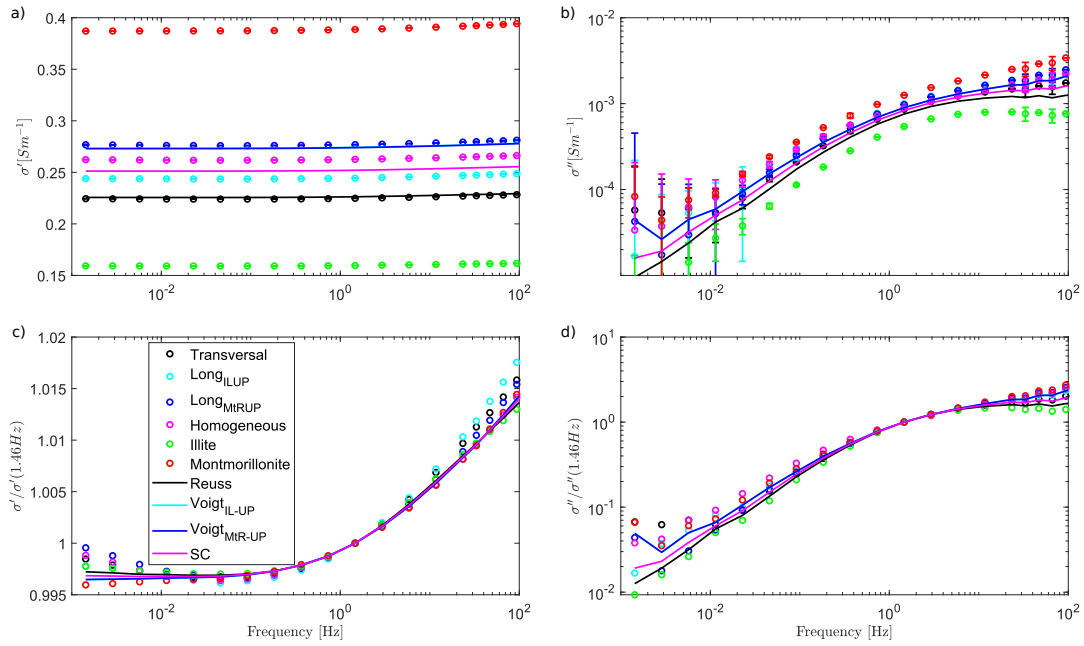


**Figure 5.** a) Real conductivity measurements, b) imaginary conductivity measurements  
 overlay by the Reuss, Voigt (IL-UP and MtR-UP), and self-consistent models, c) normalized  
 real conductivity of the measurements, and d) normalized imaginary conductivity of the mea-  
 surements overlay by the normalized Reuss, Voigt (IL-UP and MtR-UP), and self-consistent  
 models. Long<sub>IL-UP</sub> and Long<sub>MtR-UP</sub> refer to the longitudinal mixtures (parallel), with illite  
 and red montmorillonite near the potential electrodes, respectively. Reuss and Voigt refer to their  
 corresponding models, and SC corresponds to the self-consistent model. Voigt<sub>IL-UP</sub> refers to  
 a model with illite filling the half with the potential electrodes, and Voigt<sub>MtR-UP</sub> to the red  
 montmorillonite filling the half with the potential electrodes; these models are superposed.

## 5 Discussion

In this study we measured the SIP signature of a homogeneous and three heterogeneous mixtures of two types of clays, illite and red montmorillonite. The heterogeneous mixtures are arranged in a transversal and longitudinal manner. In addition to the SIP measurements, we tested the validity of traditional mixing laws and complex conductance network models to predict the resulting electrical signature of heterogeneous and homogeneous mixtures. We compared both modeling approaches to try to understand the benefits and pitfalls of each approach. Mixing laws constitute a classical approach for this kind of problems, at least for the real value component (see for instance Gueguen & Palciauskas, 1994). In this section, we discuss the difference between the two types of longitudinal measurements. We also interpret the polarization responses of the mixtures, as to which clay type is dominant. Additionally, we discuss the content of red montmorillonite in the mixtures above which the polarization is dominated by the red montmorillonite. Finally, we compare our data and modeling approaches to other approaches already published in the literature.

To better understand the reason of the difference between both longitudinal measurements, we created a numerical model (with finite elements) of the electric potential and the current density distribution within the samples (heterogeneous longitudinal mixture with montmorillonite on top, then illite on top, and finally the transversal mixture, see Fig. 6). For this numerical model, we used the COMSOL Multiphysics software to perform the numerical modeling. We created a domain with the dimensions of our sample holder, and within the domain and subdomains (top/bottom and side portions) we specified an electrical conductivity as to replicate the measurements (see Figs. 2 b, c, and d). Within COMSOL, we used the electrical currents interface which uses current conservation as the physical principle. We applied a boundary condition on the electric potential on the sides of the cylinders (see Fig. 6), and located the potential difference measurements in the exact same position as where the measuring electrodes are in the laboratory measurements. We did not use the complex nature of our measurements for this model, but it is an interesting idea for future work. We can see that there is a higher current density on the montmorillonite half, for the longitudinal samples (Figs 6a and b). This makes sense, as montmorillonite is more conductive ( $0.39 \text{ S m}^{-1}$  at 1.46 Hz) than illite ( $0.16 \text{ S m}^{-1}$  at 1.46 Hz). For the transversal sample (Fig. 6c), the current density seems unchanged from one half to the other. This also makes sense, as all the current

393 lines that pass through the montmorillonite half have to pass through the illite half. The  
 394 fact that there is a higher current density on the montmorillonite half for the longitu-  
 395 dinal arrangements could explain why we see a mismatch in the longitudinal measure-  
 396 ments (Fig. 3), for both amplitude and phase. In the first case (montmorillonite next  
 397 to the measuring electrodes) there is a higher current density on the side of the measur-  
 398 ing electrodes whereas in the second case there is less (illite next to the measuring elec-  
 399 trodes).

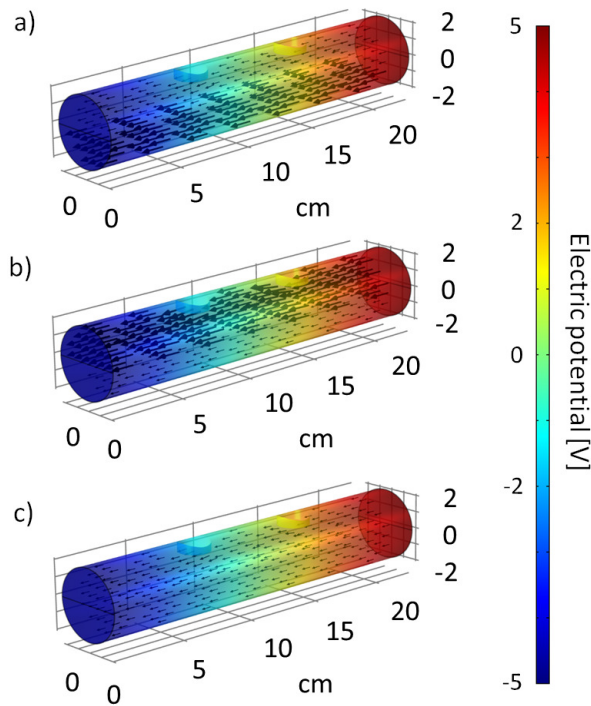


**Figure 6.** Numerical modeling of the electric potential distribution of heterogeneous clay sam-  
 ples for: a) longitudinal sample (parallel) with illite on the top portion, b) red montmorillonite  
 on the top portion and c) a transversal sample (series) with equal volumetric amounts of illite  
 and red montmorillonite. All models were subjected to an electric potential difference of -5 to 5  
 V. The arrows are a graphic representation of the current density and their size depends on the  
 amplitude of the current density.

400 An interesting result from the SIP measurements (see Fig. 3), is that the real conduc-  
 401 tivity of the mixtures is closer to the signature of the illite than the montmorillonite (in  
 402 amplitude), although the amplitude of the conductivity of the montmorillonite is larger  
 403 than that of the illite (see Fig. S5 from the supplementary information). On the other

404 hand, the shape of the spectra of the mixtures resembles more for both conductivities  
 405 (real and imaginary) the shape of the montmorillonite. That is the lack of a peak near  
 406 10 Hz for the imaginary part and an increase in the real conductivity near  $5 \times 10^2$  Hz.  
 407 As to physical explanations of this phenomenon, we could say that perhaps the specific  
 408 surface area of the montmorillonite is more important for montmorillonite than for il-  
 409 lite (from 390 to 780 m<sup>2</sup>/g according to Tournassat et al., 2013). Thus, we can think that  
 410 simply the component that polarizes the most (red montmorillonite in this case) dom-  
 411 inates the polarization of the mixtures. However, the amplitude of the conductivity will  
 412 be affected by both components of the mixture, closer to the amplitude of the conduc-  
 413 tivity of the illite, but affected by both illite and red montmorillonite nonetheless. We  
 414 would have liked to compare these results to others presented in the literature, however,  
 415 to the best of our knowledge, measurements as the ones presented in this study have not  
 416 been reported.

417 We therefore propose that, for these mixture of illite and red montmorillonite, the red  
 418 montmorillonite dominates the polarization. We wanted to test if a percolation thresh-  
 419 old exists, and if so, at which percentage of montmorillonite it lies. That is that mont-  
 420 morillonite dominates polarization as long as a certain amount is present in the mixture.  
 421 To test for this hypothesis, we performed numerical simulations of a homogeneous com-  
 422 plex conductance network with different amounts of illite; from 100% red montmorillonite,  
 423 to 10% illite, then 20%, all the way to 100% illite. The results of this test are presented  
 424 in Fig. 7. It is hard to determine where the inflexion point is, from Fig. 7 we see a smooth  
 425 transition. We cannot determine an inflexion point nor a threshold value. However, we  
 426 can say that in homogeneous mixtures of illite and montmorillonite at varying percent-  
 427 ages, the SIP signature varies smoothly.

428 We calculated the difference ( $\Delta\sigma = \sqrt{(\sigma_{model} - \sigma_{data})^2}$ ) between the models (both con-  
 429 ductance networks, and Voigt, Reuss, and self consistent models) and the measured SIP  
 430 data (see Fig. 8). We were unable to calculate a difference for the longitudinal datasets  
 431 and the conductance network models, as there is no measuring point in the complex con-  
 432 ductance network models. However, for the Voigt models, we calculated this difference  
 433 between the dataset with the illite next to the potential electrodes, and the model with  
 434 the volume fraction corresponding to that of having the space for the electrodes on its  
 435 half. We did this calculation in the same manner for the red montmorillonite, next to  
 436 the potential electrodes. This calculation determines how good the fit is, so how the val-

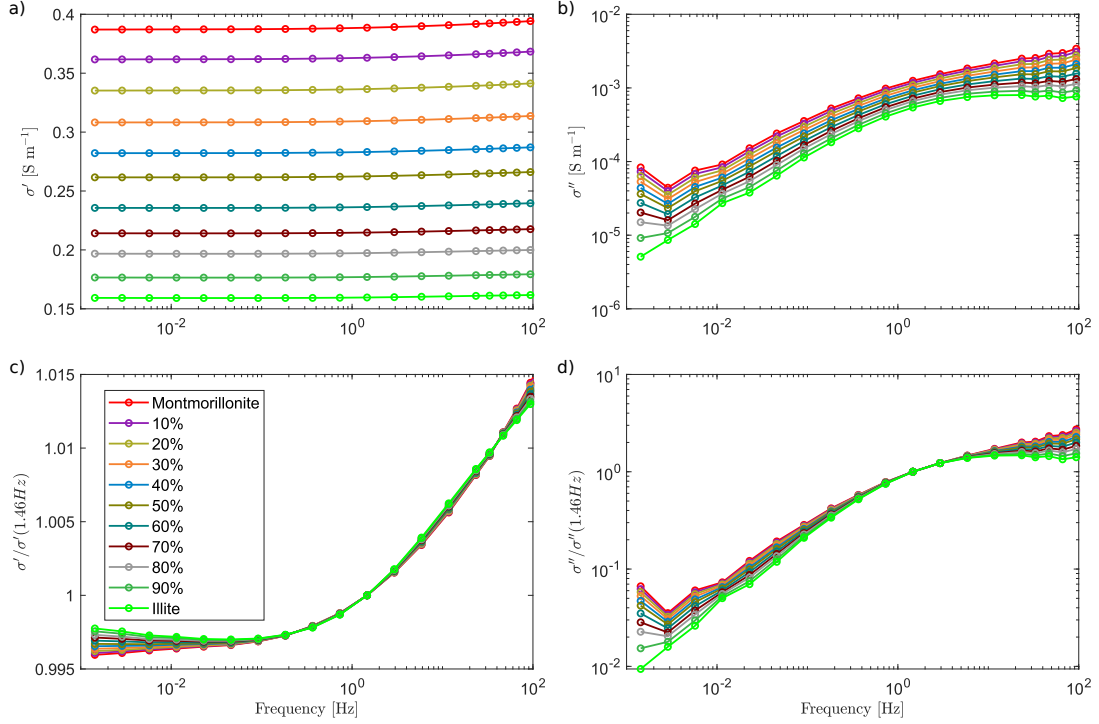


**Figure 7.** SIP modeling with complex conductance networks of a homogeneous mixture of illite and red montmorillonite, varying in illite content (from 0%, to 10%, all the way to 100%): a) real and b) imaginary part of the conductivity, c) real and d) imaginary normalized by their respective conductivities at 1.46 Hz.

437 ues of the models approached the measured data, it does not really portray how well the  
 438 model is able to predict the presence of polarization peaks at a particular frequency. For  
 439 the real part of the conductivity (Fig. 8a), definitely the Reuss, the Voigt with the red  
 440 montmorillonite next to the potential electrodes and the complex conductance network  
 441 of the homogeneous mix fit the data the best. For the imaginary part of the data (Fig.  
 442 8b), at frequencies above  $10^1$  Hz, the best fit is overall from the conductance network  
 443 approach and the Voigt model with illite next to the potential electrodes. For lower fre-  
 444 quencies, it is hard to say for the imaginary conductivity. As for the shape of the curves,  
 445 comparing Figs 4c and d, and 5c and d, it seems that the conductance network models  
 446 follow better the trend of the data, that is the presence or not of a peak at a particu-  
 447 lar frequency. Overall, we can say that the use of mixing laws for the complex conduc-  
 448 tivity is valid. Here, we make use of both the real and imaginary parts of the conduc-  
 449 tivity and the predicting capabilities of these approaches with the complex conductiv-  
 450 ity, based on Figs 5 and 8, that show a good fit between data and model. Furthermore,

451 also the use of complex conductance network models for complex conductivity seems valid,  
 452 as seen in Figs 4 and 8, also the fit between data and model are quite good.

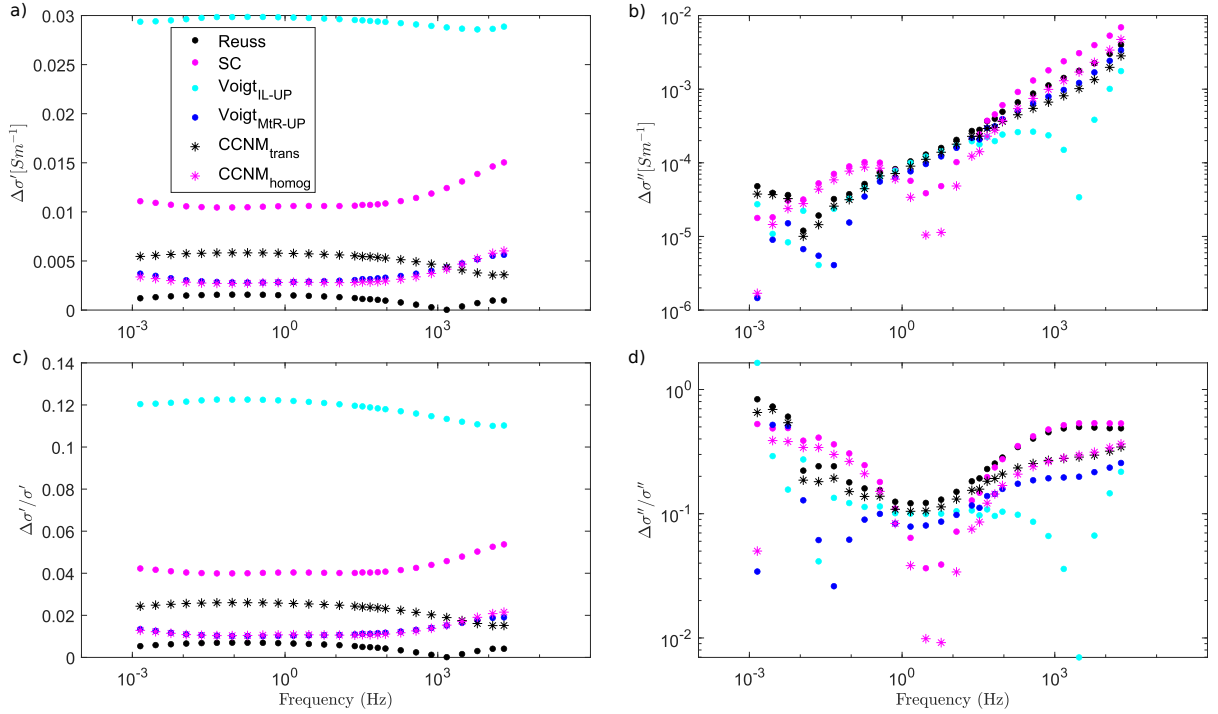


**Figure 8.** Comparison between the Reuss, Voigt, and self-consistent (SC) approach to the conductance network models, with the a) real and b) imaginary part of the electrical conductivity, c) normalized real and d) imaginary electrical conductivity.

453 One of the few studies that deal with modeling the electrical signature of anisotropic sam-  
 454 ples using impedance networks was done by Madden (1976). He created different con-  
 455 ductance networks, trying to represent different anisotropic media through pore networks,  
 456 he took a pore size distribution into account and obtained a conductivity distribution  
 457 for different scales of anisotropy in a simulated rock sample. He concludes that a geo-  
 458 metric mean of the components of the mixture is a good predictor of the physical para-  
 459 meters of a rock (electrical parameters for the purposes of this study), but this approach  
 460 does not take into account the possible complexity of the inner-connectivity of the pores  
 461 or cracks of the rock sample. This could greatly alter the resulting electrical conductiv-  
 462 ity of a rock sample. This is clearly in agreement with our results, as the Reuss and Voigt  
 463 models with the red montmorillonite next to the potential electrodes models give a bet-  
 464 ter fit to the measured real conductivity than the conductance network models (Fig. 8a).

465 Additionally, mixing laws represent a classical approach for this kind of problems, at least  
466 for the real value component (Gueguen & Palciauskas, 1994). We also agree that mod-  
467 els that do not take into account the complex connectivity of a clay sample cannot fully  
468 represent the complexity of its polarization. Here, we use the definition of anisotropy used  
469 by Lynn & Michelena (2011), which state that the measured value depends on the di-  
470 rection of the measurement itself.

471 Furthermore, Winchen et al. (2009) modeled the complex conductivity signature of a 2D  
472 anisotropic system. They suggest that anisotropy affects the electrical signature of such  
473 systems and thus it should always be taken into account. Al-Hazaimay et al. (2016) used  
474 the modeling approach of Winchen et al. (2009) and paired it with SIP measurements  
475 in the laboratory of a synthetic anisotropic system. They use a correction factor to be able  
476 to compare 2D models and 3D SIP measurements. Moreover, Al-Hazaimay et al. (2016)  
477 mention that electrical anisotropy should always be considered when performing geo-electrical  
478 measurements as they clearly affect the measured signature in the laboratory. This agrees  
479 with our observations. The use of both numerical and laboratory experiments prove to  
480 be useful to better understand the electrical signature of heterogeneous systems in both  
481 Al-Hazaimay et al. (2016) and our study. This proves that it is important to understand  
482 the small scale (laboratory scale) to be able to better interpret the field scale using geo-  
483 electrical measurements. There is still a need to bridge scale gaps from the pore to the  
484 laboratory scale and from the laboratory scale to the field scale, but we think that this  
485 study is a good step forward in that direction. Better understanding the resulting elec-  
486 trical conductivity of a mixture with a simple geometry (layering) in the laboratory will  
487 help us better understand similar structures in the field.

488 In this contribution we have presented a way to model the resulting electrical conduc-  
489 tivity of a mixture of two clays, red montmorillonite and illite, and compare it to SIP  
490 measurements of heterogeneous mixtures of clays. However, an interesting next step would  
491 be the inverse problem. Determining from a given SIP spectrum the types of clays that  
492 conform the sample, knowing what the individual SIP spectra of the components look  
493 like. Although this would prove to be a complex task, because as presented in this con-  
494 tribution, layering and volumetric content, among other elements affect the measured  
495 SIP signature of a non-consolidated clay laboratory sample.

## 6 Conclusions

We present a complex conductivity dataset of illite and red montmorillonite mixtures with equal proportions of both clays, in a parallel, perpendicular, and homogeneous manner. Our data show that the polarization of all mixtures follows rather the shape of red montmorillonite, that is lacks a polarization peak near 10 Hz distinctive of the illite sample. We interpret this as montmorillonite dominating polarization over illite. We model these mixtures through traditional mixing laws and complex conductance networks. The mixing laws are better at predicting the amplitude of the conductivity response of the mixtures, but the complex conductance models allow to better predict the presence or lack of polarization peaks at particular frequencies. Both approaches are valid to predict the electrical signature of a mixture of two types of clays. There are differences between both model approaches, as mixing laws are simple arithmetic approaches but complex conductance network models take into account somewhat the connectivity of the sample.

More work needs to be done in order to determine the percolation threshold, that is the amount of montmorillonite needed in a mixture for it to dominate the polarization of the mixture. Furthermore, this study is an advance in the bridging of the pore and laboratory scales, as the complex conductance network models have successfully allowed us to predict the resulting laboratory electrical measurement from individual pore complex conductance properties.

## Data Availability

The data used in this study is available in the zenodo repository with the doi: 10.5281/zenodo.5270269.

## Acknowledgments

The authors strongly thank the financial support of ANR EXCITING (grant ANR-17-CE06-0012) for this work and for the PhD thesis funding of A. Mendieta. We thank Jana Börner, Matthias Bücke and an anonymous reviewer for their insightful comments that helped improve the paper.

524 **References**

- 525 Al-Hazaimay, S., Huisman, J. A., Zimmermann, E., & Vereecken, H. (2016). Us-  
 526 ing electrical anisotropy for structural characterization of sediments: an ex-  
 527 perimental validation study. *Near Surface Geophysics*, *14*(4), 357–369. doi:  
 528 10.3997/1873-0604.2016026
- 529 Bairlein, K., Bucker, M., Hördt, A., & Hinze, B. (2016). Temperature depen-  
 530 dence of spectral induced polarization data: experimental results and membrane  
 531 polarization theory. *Geophysical Journal International*, *205*(1), 440–453. doi:  
 532 10.1093/gji/ggw027
- 533 Bernabe, Y. (1995). The transport properties of networks of cracks and pores. *Jour-  
 534 nal of Geophysical Research*, *100*(B3), 4231–4241. doi: 10.1029/94JB02986
- 535 Berryman, J. G. (1995). Mixture theories for rock properties. In T. J. Ahrens (Ed.),  
 536 *Rock physics & phase relations: a handbook of physical constants* (pp. 205–228).  
 537 Washington, D.C.: American geophysical union. doi: /10.1029/RF003p0205
- 538 Breede, K., Kemna, A., Esser, O., Zimmermann, E., Vereecken, H., & Huisman,  
 539 J. A. (2012). Spectral induced polarization measurements on variably sat-  
 540 urated sand-clay mixtures. *Near Surface Geophysics*, *10*(6), 479–489. doi:  
 541 10.3997/1873-0604.2012048
- 542 Bucker, M., Flores Orozco, A., Undorf, S., & Kemna, A. (2019). On the role of  
 543 Stern- and diffuse-layer polarization mechanisms in porous media. *Journal of Geo-  
 544 physical Research: Solid Earth*, *124*(6), 5656–5677. doi: 10.1029/2019JB017679
- 545 Bucker, M., & Hördt, A. (2013a). Analytical modelling of membrane polariza-  
 546 tion with explicit parametrization of pore radii and the electrical double layer.  
 547 *Geophysical Journal International*, *194*(2), 804–813. doi: 10.1093/gji/ggt136
- 548 Bucker, M., & Hördt, A. (2013b). Long and short narrow pore models for membrane  
 549 polarization. *Geophysics*, *78*, E299–E314. doi: 10.1190/GEO2012-0548.1
- 550 Cosenza, P., Ghorbani, A., Revil, A., Zamora, M., Schmutz, M., Jougnot, D., &  
 551 Florsch, N. (2008). A physical model of the low-frequency electrical polarization  
 552 of clay rocks. *Journal of Geophysical Research: Solid Earth*, *113*(B8), 1–9. doi:  
 553 10.1029/2007JB005539
- 554 Day-Lewis, F. D., Linde, N., Haggerty, R., Singha, K., & Briggs, M. A. (2017).  
 555 Pore network modeling of the electrical signature of solute transport in dual-  
 556 domain media. *Geophysical Research Letters*, *44*(10), 4908–4916. doi:

- 557 10.1002/2017GL073326
- 558 de Lima, O. A., & Sharma, M. M. (1992). A generalized Maxwell-Wagner theory for  
559 membrane polarization in shaly sands. *Geophysics*, *57*(3), 431–440. doi: 10.1190/  
560 1.1443257
- 561 Ghorbani, A., Cosenza, P., Revil, A., Zamora, M., Schmutz, M., Florsch, N., &  
562 Jougnot, D. (2009). Non-invasive monitoring of water content and textural  
563 changes in clay-rocks using spectral induced polarization: A laboratory investiga-  
564 tion. *Applied Clay Science*, *43*(3), 493–502. doi: 10.1016/j.clay.2008.12.007
- 565 Gueguen, Y., & Palciauskas, V. (1994). *Introduction to the Physics of Rocks*. Prince-  
566 ton University Press.
- 567 Hashin, Z. (1968). Assessment of the self consistent scheme approximation: conduc-  
568 tivity of particulate composites. *Journal of Composite Materials*, *2*(3), 284–300.  
569 doi: 10.1177/002199836800200302
- 570 Hayley, K., Bentley, L. R., Gharibi, M., & Nightingale, M. (2007). Low temperature  
571 dependence of electrical resistivity: Implications for near surface geophysical moni-  
572 toring. *Geophysical Research Letters*, *34*(18), 1–5. doi: 10.1029/2007GL031124
- 573 Iravani, M. A., Deparis, J., Davarzani, H., Colombano, S., Guérin, R., & Mainault,  
574 A. (2020). The influence of temperature on the dielectric permittivity and  
575 complex electrical resistivity of porous media saturated with DNAPLs: A lab-  
576 oratory study. *Journal of Applied Geophysics*, *172*, 1–11. doi: 10.1016/  
577 j.jappgeo.2019.103921
- 578 Jougnot, D. (2020). *Developing hydrogeophysics for critical zone studies, importance*  
579 *of heterogeneities and processes at the mesoscopic scale* (Habilitation dissertation,  
580 Sorbonne Université, Paris, France). doi: 10.5281/zenodo.5517748
- 581 Jougnot, D., Ghorbani, A., Revil, A., Leroy, P., & Cosenza, P. (2010). Spectral in-  
582 duced polarization of partially saturated clay-rocks: a mechanistic approach. *Geo-*  
583 *physical Journal International*, *180*(1), 210–224. doi: 10.1111/j.1365-246X.2009  
584 .04426.x
- 585 Jougnot, D., Jiménez-Martínez, J., Legendre, R., Le Borgne, T., Méheust, Y., &  
586 Linde, N. (2018). Impact of small-scale saline tracer heterogeneity on electri-  
587 cal resistivity monitoring in fully and partially saturated porous media: Insights  
588 from geoelectrical milli-fluidic experiments. *Advances in Water Resources*, *113*,  
589 295–309. doi: 10.1016/j.advwatres.2018.01.014

- 590 Jougnot, D., Mendieta, A., Leroy, P., & Maineult, A. (2019). Exploring the effect  
591 of the pore size distribution on the streaming potential generation in saturated  
592 porous media, insight from pore network simulations. *Journal of Geophysical*  
593 *Research: Solid Earth*, *124*(6), 5315–5335. doi: 10.1029/2018JB017240
- 594 Kemna, A., Binley, A., Cassiani, G., Niederleithinger, E., Revil, A., Slater, L., ...  
595 Zimmermann, E. (2012). An overview of the spectral induced polarization method  
596 for near-surface applications. *Near Surface Geophysics*, *10*(6), 453–468. doi:  
597 10.3997/1873-0604.2012027
- 598 Kenkel, J., Hördt, A., & Kemna, A. (2012). 2D modelling of induced polarization  
599 data with anisotropic complex conductivities. *Near Surface Geophysics*, *10*(6),  
600 533–544. doi: 10.3997/1873-0604.2012050
- 601 Kirchhoff, G. (1845). Ueber den Durchgang eines elektrischen Stromes durch eine  
602 Ebene, insbesondere durch eine kreisförmige. *Annalen der physik und chemie*,  
603 *140*, 497–514. doi: 10.1002/andp.18451400402
- 604 Knight, R. J., & Endres, A. L. (2005). An introduction to rock physics principles  
605 for near-surface geophysics. In D. K. Butler (Ed.), *Near-surface geophysics* (pp.  
606 31–65). Tulsa, Oklahoma: Society of Exploration Geophysicists. doi: 10.1190/1  
607 .9781560801719.ch3
- 608 Kremer, T., Schmutz, M., Maineult, A., & Agrinier, P. (2016). Laboratory mon-  
609 itoring of CO<sub>2</sub> injection in saturated silica and carbonate sands using spectral  
610 induced polarization. *Geophysical Journal International*, *207*(2), 1258–1272. doi:  
611 10.1093/gji/ggw333
- 612 Leroy, P., Weigand, M., Mériguet, G., Zimmermann, E., Tournassat, C., Fager-  
613 lund, F., ... Huisman, J. A. (2017). Spectral induced polarization of Na-  
614 montmorillonite dispersions. *Journal of Colloid And Interface Science*, *505*,  
615 1093–1110. doi: 10.1016/j.jcis.2017.06.071
- 616 Loewer, M., Günther, T., Igel, J., Kruschwitz, S., Martin, T., & Wagner, N. (2017).  
617 Ultra-broad-band electrical spectroscopy of soils and sediments—a combined per-  
618 mittivity and conductivity model. *Geophysical Journal International*, *210*(3),  
619 1360–1373. doi: 10.1093/gji/ggx242
- 620 Lynn, H., & Michelena, R. J. (2011). Introduction to this special section: Practi-  
621 cal applications of anisotropy. *The Leading Edge*, *30*(7), 726–730. doi: 10.1190/1  
622 .3609086

- 623 Madden, T. R. (1976). Random networks and mixing laws. *Geophysics*, *41*(6 A),  
624 1104–1125. doi: 10.1190/1.2035907
- 625 Maineult, A. (2018a). Corrigendum to “Upscaling of spectral induced polarization  
626 response using random tube networks”, by Maineult et al. (2017, *Geophysical*  
627 *Journal International*, 209, pp. 948–960). *Geophysical Journal International*, *213*,  
628 1296–1296. doi: 10.1093/gji/ggy052
- 629 Maineult, A., Gurin, G., & Titov, K. (2021). Impedance network modelling to sim-  
630 ulate the chargeability of sand-pyrite mixtures. In *27th european meeting of envi-*  
631 *ronmental and engineering geophysics* (pp. 1–5). Bordeaux, France: European As-  
632 sociation of Geoscientists and Engineers. doi: 10.3997/2214-4609.202120050
- 633 Maineult, A., Jougnot, D., & Revil, A. (2018b). Variations of petrophysical proper-  
634 ties and spectral induced polarization in response to drainage and imbibition: A  
635 study on a correlated random tube network. *Geophysical Journal International*,  
636 *212*, 1398–1411. doi: 10.1093/gji/ggx474
- 637 Maineult, A., Revil, A., Camerlynck, C., Florsch, N., & Titov, K. (2017). Upscaling  
638 of spectral induced polarization response using random tube networks. *Geophysi-*  
639 *cal Journal International*, *209*, 948–960. doi: 10.1093/gji/ggx066
- 640 Mendieta, A., Jougnot, D., Leroy, P., & Maineult, A. (2021). Spectral induced  
641 polarization characterization of non-consolidated clays for varying salinities - an  
642 experimental study. *Journal of Geophysical Research: Solid Earth*, *126*(4). doi:  
643 10.1029/2020jb021125
- 644 Okay, G., Leroy, P., Ghorbani, A., Cosenza, P., Camerlynck, C., Cabrera, J., ... Re-  
645 vil, A. (2014). Spectral induced polarization of clay-sand mixtures : Experiments  
646 and modeling. *Geophysics*, *79*(6), 353–375. doi: 10.1190/geo2013-0347.1
- 647 Pelton, W., Ward, S. H., Hallof, P. G., Sill, W. R., & Nelson, P. H. (1978). Mineral  
648 discrimination and removal of inductive coupling with multifrequency IP. *Geophy-*  
649 *ics*, *43*(3), 588–609. doi: 10.1190/1.1440839
- 650 Pride, S. (1994). Governing equations for the coupled electromagnetics and acoustics  
651 of porous media. *Physical Review B*, *50*(21), 15678–15696.
- 652 Renard, P., & de Marsily, G. (1997). Calculating equivalent permeability:  
653 a review. *Advances in Water Resources*, *20*(5-6), 253–278. doi: 10.1016/  
654 S0309-1708(96)00050-4.
- 655 Reuss, A. (1929). Berechnung der Fließgrenze von Mischkristallen auf Grund der

- 656 Plastizitätsbedingung für Einkristalle. *Zeitschrift für Angewandte Mathematik und*  
657 *Mechanik*, 9(1), 49–58. doi: 10.1002/zamm.19290090104
- 658 Revil, A. (2012). Spectral induced polarization of shaly sands: Influence of the  
659 electrical double layer. *Water Resources Research*, 48(2), 1–23. doi: 10.1029/  
660 2011WR011260
- 661 Revil, A., Linde, N., Cerepi, A., Jougnot, D., Matthäi, S., & Finsterle, S. (2007).  
662 Electrokinetic coupling in unsaturated porous media. *Journal of Colloid and*  
663 *Interface Science*, 313(1), 315–327. doi: 10.1016/j.jcis.2007.03.037
- 664 Revil, A., Woodruff, W. F., Torres-Verdín, C., & Prasad, M. (2013). Complex  
665 conductivity tensor of anisotropic hydrocarbon-bearing shales and mudrocks.  
666 *Geophysics*, 78(6), E299–E314. doi: 10.1190/GEO2012-0548.1
- 667 Stebner, H., Halisch, M., & Hördt, A. (2017). Simulation of membrane polarization  
668 of porous media with impedance networks. *Near Surface Geophysics*, 15(6), 563–  
669 578. doi: 10.3997/1873-0604.2017054
- 670 Tournassat, C., Grangeon, S., Leroy, P., & Giffaut, E. (2013). Modeling specific pH  
671 dependent sorption of divalent metals on montmorillonite surfaces. A review of  
672 pitfalls, recent achievements and current challenges. *American Journal of Science*,  
673 313(5), 395–451. doi: /10.2475/05.2013.01
- 674 Voigt, W. (1910). *Lehrbuch der Kristallphysik*. Leipzig, Germany: Teubner-Verlag.
- 675 Wenk, H. R., Voltolini, M., Mazurek, M., Van Loon, L. R., & Vinsot, A. (2008).  
676 Preferred orientations and anisotropy in shales: Callovo-oxfordian shale (France)  
677 and opalinus clay (Switzerland). *Clays and Clay Minerals*, 56(3), 285–306. doi:  
678 10.1346/CCMN.2008.0560301
- 679 Winchen, T., Kemna, A., Vereecken, H., & Huisman, J. A. (2009). Characterization  
680 of bimodal facies distributions using effective anisotropic complex resistivity : A  
681 2D numerical study based on Cole-Cole models. *Geophysics*, 74(3), A19–A22. doi:  
682 10.1190/1.3113986
- 683 Woodruff, W. F., Revil, A., & Torres-Verdín, C. (2014). Laboratory determina-  
684 tion of the complex conductivity tensor of unconventional anisotropic shales. *Geo-*  
685 *physics*, 79(5), E183–E200. doi: 10.1190/geo2013-0367.1
- 686 Zanetti, C., Weller, A., Vennetier, M., & Mériaux, P. (2011). Detection of buried  
687 tree root samples by using geoelectrical measurements: A laboratory experiment.  
688 *Plant Soil*, 339(1), 273–283. doi: 10.1007/s11104-010-0574-0

- 689 Zimmermann, E., Kemna, A., Berwix, J., Glaas, W., Münch, H. M., & Huisman,  
690 J. A. (2008). A high-accuracy impedance spectrometer for measuring sediments  
691 with low polarizability. *Measurement Science and Technology*, *19*(10), 1–9. doi:  
692 10.1088/0957-0233/19/10/105603
- 693 Zisser, N., Kemna, A., & Nover, G. (2010). Dependence of spectral-induced polar-  
694 ization response of sandstone on temperature and its relevance to permeability  
695 estimation. *Journal of Geophysical Research: Solid Earth*, *115*(9), 1–15. doi:  
696 10.1029/2010JB007526